

## RADIATIVE RECOMBINATION DATA FOR MODELLING DYNAMIC FINITE-DENSITY PLASMAS

N. R. BADNELL

Department of Physics, University of Strathclyde, Glasgow G4 0NG, UK  
*Draft version April 8, 2006*

### ABSTRACT

We have calculated partial final-state resolved radiative recombination (RR) rate coefficients from the initial ground and metastable levels of all elements up to and including Zn, plus Kr, Mo, and Xe, for all isoelectronic sequences up to Na-like forming Mg-like. The data are archived according to the Atomic Data and Analysis Structure (ADAS) data class *adf48*, which spans a temperature range of  $z^2(10^1 - 10^7)$  K, where  $z$  is the initial ion charge. Fits to total rate coefficients have been determined, for both the ground and metastable levels, and those for the ground are presented here. Comparison is made both with previous RR rate coefficients and with (background)  $R$ -matrix photoionization cross sections. This RR database complements a DR database already produced and both are being used to produce updated ionization balances for both (electron) collisionally ionized and photoionized plasmas.

*Subject headings:* atomic data – atomic processes – plasmas

### 1. INTRODUCTION

Astrophysical and laboratory plasmas which are not in (local) thermodynamic equilibrium require a detailed modelling of their atomic and, sometimes, molecular reactions so as to determine the level populations and ionization balance of their constituents. These in turn are basic ingredients for the physical and spectral diagnostic modelling of stellar coronae, gaseous nebulae, supernova remnants, fusion plasmas, etc. At low particle densities, e.g. the ‘coronal approximation’, ionization balance is between total groundstate dielectronic-plus-radiative recombination and groundstate ionization by electrons and/or photons, while level populations are determined by collisional excitation from the groundstate and radiation to all possible lower states. As the particle density increases, a separation between the two is no longer possible and level populations, effective recombination & ionization rate coefficients and ionization balance are determined by solving the collisional–radiative population rate equations (Bates et al. 1962; Burgess & Summers 1969; Summers et al. 2006). Furthermore, even at the low densities found in gaseous nebulae, for example, the populations of ions of C, N, O which have fine-structure levels in their ground term are not concentrated in the ground level. Recombination from excited levels within the ground term is quite different (smaller) compared to that for the ground level, due to the presence of additional autoionization pathways. Furthermore, transient plasmas such as solar flares do not have time to establish quasi-static equilibrium with the ground level and so require metastable levels (and the excited-state populations built upon them) to be treated on an equal footing as the ground level when it comes to collisional–radiative modelling (Summers & Hooper 1983).

However, historically, total (zero-density) ground state recombination rate coefficients have dominated the literature — see, for example, those used by Shull & van Steenberg (1982); Arnaud & Rothenflug (1985); Péquignot et al. (1991); Arnaud & Raymond (1992); Mazzotta et al. (1998). A systematic attempt to move beyond this picture has been described by

Badnell et al. (2003), who focussed on dielectronic recombination but much of the discussion there is applicable to radiative recombination — deliberately so. Now, using AUTOSTRUCTURE (Badnell 1986), we have calculated partial final-state resolved radiative recombination (RR) rate coefficients from the initial ground and metastable levels of all elements up to and including Zn, plus Kr, Mo and Xe, for all isoelectronic sequences up to Na-like forming Mg-like. The data are archived according to the Atomic Data and Analysis Structure (ADAS) data class *adf48*<sup>1</sup> (Summers 2005). Fits to total RR rate coefficients have been determined, for both the ground and metastable levels, and those for the ground are presented here. All of the data are available online (Badnell 2006b), along with corresponding data for DR (Badnell 2006a).

Previous work on RR has been summarized by Mazzotta et al. (1998). Since then, Gu (2003b) has presented RR rate coefficients obtained using his Flexible Atomic Code FAC for Mg, Si, S, Ar, Ca, Fe, and Ni, for all isoelectronic sequences through to F-like forming Ne-like.

The time reversed process of RR (plus DR) is photoionization (PI), indeed, our RR is determined from our direct photoionization cross sections on using the principle of detailed balance. We make comparison of our groundstate-to-groundstate photoionization cross sections of neutral atoms with those obtained from various  $R$ -matrix calculations, by others, as the most severe test of our results. Similar  $R$ -matrix data has been used by Nahar and co-workers (e.g., Nahar 1999) to form total (DR+RR) rate coefficients, and we make a comparison with it by combining our RR data with complementary DR data (Badnell 2006a).

The remainder of the paper is organized as follows: in Section 2 we describe our methodology, in Section 3 we present our results and make comparisons with the results of earlier works, and then make some concluding

<sup>1</sup> The historic ADAS dataclass file for RR is *adf08* but it is structured to handle RR to low-lying levels only, so as to supplement their population by electron-impact excitation.

remarks.

## 2. METHODOLOGY

### 2.1. Theory

We use the independent processes approximation so as to treat RR and DR separately. Interference between DR resonances and the RR background can safely be neglected, especially on integrating over resonance profiles (Pindzola et al. 1992). We use AUTOSTRUCTURE (Badnell 1986) to calculate multi-configuration intermediate-coupling distorted-wave photoionization cross sections (Badnell & Seaton 2003). These are converted to RR cross sections using detailed balance. For elements beyond Zn we use semi-relativistic radial functions in place of the non-relativistic ones used up until then (Pindzola & Badnell 1990).

### 2.2. Atomic Details

For each sequence, we used the same set of initial and final configurations as was done for ( $\Delta n = 0$ ) DR (Badnell et al. 2003), i.e., we included configuration mixing in the initial  $N$ -electron, and final  $N$ - or  $(N + 1)$ -electron complexes for RR outwith or into the initial complexes, respectively. Each inequivalent  $nl$  electron-state was treated separately. Radial functions were determined using the Slater-Type-Orbital model potential option of AUTOSTRUCTURE, which generates (slightly, in this case) non-orthogonal orbitals. We follow Cowan (1981) in not imposing orthogonality and assuming the overlaps to be zero or unity, as appropriate. This is more of an issue for inner-shell photoionization where large relaxation effects occur for L-shell orbitals following K-shell photoionization, see e.g., Gorczyca et al. (2006a). For recombination/ionization to/from the ground complex we used the observed ionization potentials from NIST (v3). Energy adjustments were made to the diagonal of the  $LS$ -coupling Hamiltonian before recoupling to, and diagonalization of, the intermediate coupling Hamiltonian. Finally, to determine total RR and/or DR rate coefficients we sum over only final states which are stable against autoionization.

### 2.3. Numerics

Cross sections were calculated at zero electron energy and then on a  $z$ -scaled logarithmic energy mesh with 3-points per decade spanning  $(2.1 \times 10^{-6} - 1 \times 10^2)z^2$  Ryd, where  $z$  is the charge of the ion before/after recombination/photoionization. Tests were also made using 5-points per decade. The length gauge is used at low energies, progressively and automatically switching to velocity and then acceleration as the energy increases so as to maintain numerical accuracy, but not before the succeeding gauge has converged to the preceding one. Cross sections at higher energies were determined by extrapolation as  $E^{-l-7/2}$  (for PI), where  $l$  is the orbital angular momentum of the bound orbital. Rate coefficients were determined over  $(10^1 - 10^7)z^2$  K and so are not particularly sensitive to the exact form used for the extrapolation of the cross sections. With many thousands of individual partial rate coefficients to be determined, a fast and accurate Maxwellian convolution method is desirable. We use a variant of that due to Burgess (1964), viz., a 5-point Newton-Coates quadrature on a doubling energy

mesh, with a 4-point Lagrange interpolation formula to convert from the initial logarithmic energy mesh, completed by an exponential integral. By using a  $z$ -scaled minimum temperature we can use a fixed maximum value for the principal quantum number, viz., 1000, and orbital angular momentum, viz., 200. We use analytic hydrogenic radial integrals for  $l \geq 4$  making, use of the fast, accurate, recurrence relations of Burgess (1964). All resultant partial RR rate coefficients are designed to be numerically accurate to 3 significant figures.

### 2.4. Database Details

The processing of photoionization cross sections from AUTOSTRUCTURE is carried-out using the ADASRR code. The output of ADASRR is similar in nature to the ADASDR code used for DR (Badnell et al. 2003), i.e. the ADAS *adf48* file which it writes for RR is very similar in structure to the *adf09* file for DR (Summers 2005). Viz., for each initial level (ground-plus-metastables) there is a progressive bundling over final outer quantum numbers as  $n$  increases. Partial RR rate coefficients to low-lying levels (those with  $n \leq 8$ ) are fully  $J$ -resolved, then bundled- $nl$  ( $n \leq 10$ ) and bundled- $n$  ( $n < 1000$ ), but each with a fully  $J_c$ -resolved core. Finally, total RR rate coefficients are written for each specified initial ground and metastable level. The full set of RR data — partials (*adf48* files) and totals (fit coefficients) — is available online (Badnell 2006b), alongside the DR data (Badnell 2006a), and it is also part of the ADAS distribution. (OPEN\_ADAS, a public access version of ADAS is scheduled to come online in the Summer of 2006, sponsored and hosted by the International Atomic Energy Agency.)

### 2.5. The Fit

Total RR rate coefficients, for both ground and metastable initial levels, are fitted to the usual functional form (Verner & Ferland 1996; Gu 2003b) viz.

$$\alpha_{\text{RR}}(T) = A \times \left[ \sqrt{T/T_0} \left(1 + \sqrt{T/T_0}\right)^{1-B} \left(1 + \sqrt{T/T_1}\right)^{1+B} \right]^{-1}, \quad (1)$$

where, for low-charge ions,  $B$  is replaced as

$$B \rightarrow B + C \exp(-T_2/T). \quad (2)$$

Here,  $T_{0,1,2}$  are in units of temperature (K) and the rate coefficient  $\alpha_{\text{RR}}(T)$  is in units of  $\text{cm}^3 \text{s}^{-1}$ . (The units of  $A$  are also  $\text{cm}^3 \text{s}^{-1}$ , while  $B$  and  $C$  are dimensionless.) A non-linear least-squares fit was used to determine the coefficients ( $A, B, T_{0,1}; C, T_2$ ). The fits are accurate to better than 1% over  $(10^1 - 10^7)z^2$  K for multiply charged ions, 5% for singly and doubly ionized, and have the correct asymptotic forms outside of this range.

## 3. RESULTS

Fit coefficients according to Equations (1) and (2) are presented in Table 1 for total groundstate RR rate coefficients for all elements up to and including Zn, plus Kr, Mo and Xe, for all isoelectronic sequences up to Na-like forming Mg-like. Partial final-state resolved RR rate coefficients for initial ground and metastable levels are archived as ADAS *adf48* files (Summers 2005). Fits to total RR rate coefficients have been determined for initial metastable levels as well. All of the data are available online (Badnell 2006b), along with corresponding data for DR (Badnell 2006a).

### 3.1. Photoionization Cross Sections

The description of groundstate-to-groundstate photoionization of neutral atoms provides the most stringent test of the accuracy of our description of partial and high-temperature-total RR rate coefficients.

In Figure 1 we compare photoionization cross sections of neutral O for the transition  $O(^3P) \rightarrow O^+(^4S)$ . We see that our AUTOSTRUCTURE results closely track the background  $R$ -matrix cross sections of Butler & Zeppen (1990), to within 7%.

In Figure 2 we make a similar comparison for neutral Na. This is an interesting system since it features a Cooper minimum (Fano & Cooper 1968). We see that our AUTOSTRUCTURE photoionization cross sections give a reasonable description of this feature, on comparison with the  $R$ -matrix results of Butler & Mendoza (1983); TOPbase, Cunto et al. (1993).

Finally, in Figure 3 we look at the high energy behaviour of the  $Mg^+$  photoionization cross section: we compare our energy-scaled AUTOSTRUCTURE cross sections with the Dirac–Hartree–Slater results of Verner & Yakovlev (1995). We see that at the high energy cross sections of Verner & Yakovlev (1995) have still to reach their asymptotic form, of  $E^{-7/2}$ . Analysis of the fitting form and parameters of Verner & Yakovlev (1995) shows that it will not reach asymptopia until  $\sim 10^6$  Ryd, which appears unphysically high. Similar disagreement is seen in other low-charge Na-like ions, the effect decreasing with increasing residual charge.

### 3.2. Total Groundstate Rate Coefficients

In Figures 4 and 5 we illustrate an overview of total groundstate RR rate coefficients, viz. the Mg isonuclear sequence and the F isoelectronic sequence. The change in behaviour on moving from K- to L- and then M-shells is clearly seen in the former and the characteristic high-temperature bump at low-charges in the latter.

In Figure 6 we compare our F-like Ne and Mg rate coefficients from AUTOSTRUCTURE with those of Péquignot et al. (1991) and Gu (2003b), respectively. The high-temperature limit on the validity of the simple functional form used by Péquignot et al. (1991) is a few times  $10^4$  K, but DR dominates thereon. The more general form, given by Equations (1) and (2), does not suffer from this limitation. The comparison with the results of Gu (2003b) for Mg illustrates the worst agreement found with his work, viz., about 10% in the vicinity of  $5 \times 10^4$  K, and up to 20% at  $10^8$  K.

In Figure 7 we compare our Ne-like Na and Mg rate coefficients from AUTOSTRUCTURE with those of Verner & Ferland (1996). The latter are based on Opacity Project (TOPbase, Cunto et al. 1993)  $R$ -matrix background photoionization cross sections at low energies and the Dirac–Hartree–Slater ones of Verner & Yakovlev (1995) at higher energies. We have already seen the agreement between our low energy (groundstate) neutral Na photoionization cross sections and those from  $R$ -matrix — those for  $Mg^+$  show good agreement as well (not shown). We noted also that the high energy Dirac–Hartree–Slater results lie *above* those from AUTOSTRUCTURE. But, here, we see that the high temperature RR rate coefficients of Verner & Ferland (1996) lie *below* our results — RR into the 3s dominates at high temperatures

— which is puzzling. However, the rise of DR at  $10^5$  K postpones significant disagreement in the (DR+RR) total until  $\sim 10^7$  K.

In Figure 8 we compare our  $Mg^+$  rate coefficients from AUTOSTRUCTURE with the RR of Aldrovandi & Péquignot (1973) (and used again by Shull & van Steenberg 1982, without modification) and which still form the basis of recommended data for this ion (Mazzotta et al. 1998). Our RR results are 70% and a factor of 3 larger at  $10^3$  and  $10^4$  K, respectively, but DR dominates at the latter temperature while it is negligible at the former. The results of Aldrovandi & Péquignot (1973) make use of very restricted (near-threshold) photoionization cross section measurements by Ditchburn & Marr (1953). This new rate coefficient changes the ionization balance of Mg in many photoionized plasmas, and affects Mg II emissivities noticeably (Ferland 2006), for example.

Finally, in Figure 9 we compare total (DR+RR) rate coefficients from AUTOSTRUCTURE for  $O^{2+}$  with the  $R$ -matrix results of Nahar (1999). We also show separately the contribution from the present RR rate coefficients and the DR ones of Zatsarinny et al. (2004a), taken from Badnell (2006a). At the high temperature peak ( $2 \times 10^5$  K) the results of Nahar (1999) lie about 8% above the present ones, and remain constantly so thereon. Below about  $2 \times 10^4$  K the contribution from fine-structure DR separates the two results. The calculations of Nahar (1999) were carried-out in  $LS$ -coupling and so this is absent and her results track our RR results to within a few percent.

### 3.3. Total Metastable Rate Coefficients

In Figure 10 we present total rate coefficients from the ground and metastable levels of  $O^{2+}$  ( $^3P_{0,1,2}, ^1D_2, ^1S_0, ^5S_2$ ). Fine structure splitting in the  $^3P_J$  ground term only starts to affect RR at very low temperatures ( $\sim 30\%$  at 100 K). This is in contrast to DR where the lower two levels are strongly enhanced by the fine-structure pathway(s) open to them while the upper level only has a small low temperature peak which never exceeds the RR contribution. RR onto excited terms is reduced distinctly by autoionization, compared to that for levels within a term. The  $^1D_2$  and  $^1S_0$  contributions are similarly sized, both for RR and the high temperature DR peak (at  $10^5$  K). The  $^5S_2$  RR contribution is the smallest but its high temperature DR peak exceeds that of the  $^1D_2$  and  $^1S_0$  initial states. The widely varying behaviours of DR and RR for ground and metastable levels is then reflected similarly in the temperature dependence of the (DR+RR) total recombination rate coefficients (not shown).

### 3.4. Partial Rate Coefficients

In Figures 11 and 12 we compare partial final-state resolved rate coefficients for recombination from the initial ground state of  $O^{2+}$  to the  $2s^2 2p^3 ^4S_{3/2}$  and  $2s^2 2p^2 3p^4 D_J$  states of  $O^+$ , respectively, where we have summed-over the fine-structure  $J$  of the  $^4D$  term, for convenience of comparison. The DR is taken from the partial *adf09* files of Zatsarinny et al. (2004a), archived by Badnell (2006a). As in the case of totals, we see that the partial DR is enhanced below  $\sim 1000$  K by fine-structure transitions. The ( $LS$ -coupling)  $R$ -matrix results of Nahar

(1999) lie 15% and 35% below our RR results for the ground and excited state, respectively, at temperatures below  $\sim 1000$  K.

Recombination into the  $2s^22p^23p^4D_J$  states of  $O^+$  is of interest because of the discrepancy in temperatures needed to model recombination line and forbidden line abundances in the Ring Nebula NGC 6720 (Garnett & Dinerstein 2001). The relevant recombination line (emissivity) is for the subsequent  $3p^4D$  to  $3s^4P$  transition at  $\lambda 4661$  in OII. The  $\lambda 4661$  emissivity used by Garnett & Dinerstein (2001) is based-on the effective recombination rate coefficient of Storey (1994), whose calculations were carried-out in *LS*-coupling. We note (not shown) only a  $\approx 10\%$  enhancement of the zero-density non-cascade partial sum (RR+DR) at  $10^4$  K, on going from *LS*- to intermediate-coupling. This enhancement becomes a factor of two down at  $10^3$  K, but it is probably too low a temperature to help resolve the discrepancy in the Ring Nebula. Interestingly, our partial sum (DR+RR) rate coefficient to  $2s^22p^23p^4D$  agrees to about 10% with the  $\lambda 4661$  effective recombination rate coefficient of Storey (1994), over the temperature range of  $5 \times 10^3 - 2 \times 10^4$  K for which he tabulates results. Since density effects are negligible for this line and the branching ratio for  $3p^4D$  to  $3s^4P$  is approximately unity, we infer that the cascade correction is not large. Work

on a detailed revised  $\lambda 4661$  effective recombination rate coefficient is in progress (Storey 2006).

#### 4. CONCLUDING REMARKS

We have outlined the database of RR rate coefficients which we have established using AUTOSTRUCTURE. Although we have highlighted some differences from previous results which we have observed, the bulk of the groundstate total data is in good accord with the extant. It is hoped that the availability of comprehensive partial final-state resolved and metastable totals will stimulate the advanced modelling of non-equilibrium astrophysical plasmas, viz., dynamic, finite-density. Together with complementary data for DR, new ionization balances are already being determined for both (electron) collisional (Bryans et al. 2006) and photoionized (Ferland 2006) plasmas.

I would like to thank Randall Smith and Daniel Péquignot for their interest in the partial and metastable RR rate coefficients, respectively. I would also like to thank Keith Butler for supplying his *R*-matrix photoionization cross sections of O in numerical form. This work was supported in part by PPARC Grant No. PPA\G\S2003\00055 with the University of Strathclyde.

#### REFERENCES

- Aldrovandi, S. M. V., & Péquignot, D. 1973 A&A, 25, 137  
 Altun, Z., Yumak, A., Badnell, N.R., Loch, S.D., & Pindzola, M.S. 2006, A&A, 447, 1165  
 Arnaud, M., & Raymond, J. C. 1992, ApJ, 398, 394  
 Arnaud, M., & Rothenflug, R. 1985, A&AS, 60, 425  
 Badnell, N. R. 1986, J. Phys. B, 19, 3827  
 Badnell, N. R. 2006a, <http://amdpp.phys.strath.ac.uk/tamoc/DR/>  
 Badnell, N. R. 2006b, <http://amdpp.phys.strath.ac.uk/tamoc/RR/>  
 Badnell, N. R., O'Mullane, M. G., Summers, H. P., Altun, Z., Bautista, M. A., Colgan, J., Gorczyca, T. W., Mitnik, D. M., Pindzola, M. S., & Zatsarinny, O. 2003, A&A, 406, 1151  
 Badnell, N. R., & Seaton, M. J. 2003, J. Phys. B, 36, 4367  
 Bates, D. R., Kingston, A. E., & McWhirter, R. W. P. 1962, Proc. Roy. Soc. A, 267, 297  
 Bryans, P., Badnell, N. R., Gorczyca, T. W., Laming, J. M., Mitthumsiri, W., & Savin, D. W. 2006, ApJS, To be submitted  
 Burgess, A. 1964, Mem. Roy. Astr. Soc., 69, 1  
 Burgess, A., & Summers, H. P. 1968, ApJ, 157, 1007  
 Butler, K., & Mendoza, C. 1983, J. Phys. B, 16, L707  
 Butler, K., & Zeippen, C. J. 1990, A&A, 234, 569  
 Cowan, R. D. 1981, The Theory of Atomic Structure and Spectra (Berkeley: Univ. California Press)  
 Cunto, W., Mendoza, C., Ochsenbein, F., & Zeippen, C. J. 1993, A&A, 275, L5  
<http://vizier.u-strasbg.fr/topbase/topbase.html>  
 Ditchburn, R. W., & Marr, G. V. 1953, Proc. Phys. Soc. A, 66, 665  
 Fano, U., & Cooper, J. W. 1968, Rev. Mod. Phys., 40, 441  
 Ferland, G. J. 2006, Private Communication  
 Garnett, D. R., & Dinerstein, H. L. 2001, ApJ, 558, 145  
 Gorczyca, T. W., Dumitriu, I., Hasoğlu, Korista, K. T., Badnell, N. R., Savin, D. W., & Manson, S. T. 2006, ApJ, 638, L121  
 Gorczyca, T. W., et al. 2006, Phys. Rev. A, To be Submitted  
 Gu, M. F. 2003b, ApJ, 589, 1085  
 Mazzotta, P., Mazzitelli, G., Colafrancesco, S., & Vittorio, N. 1998, A&AS, 133, 403  
 Nahar, S. N. 1999, ApJS, 120, 131  
 NIST Atomic Spectral Database v3  
<http://physics.nist.gov/PhysRefData/ASD>  
 Péquignot, D., Petitjean, P., & Boisson, C. 1991, A&A, 251, 680  
 Pindzola, M. S., & Badnell, N. R. 1990, Phys. Rev. A, 42, 6526  
 Pindzola, M. S., Badnell, N. R., & Griffin, D. C. 1992, Phys. Rev. A, 46, 5725  
 Shull, J. M., & van Steenberg, M. 1982, ApJS, 48, 95; erratum 1982, ApJS, 49, 351  
 Storey, P. J. 1994, A&A, 282, 999  
 Storey, P. J. 2006, Private Communication  
 Summers, H. P., & Hooper, M. B. 1983, Plasma Phys. Control. Fusion, 44, B323  
 Summers, H. P. 2005, ADAS Manual v2.7  
<http://adas.phys.strath.ac.uk>  
 Summers, H. P. et al. 2006, Plasma Phys. Control. Fusion, 48, 263  
 Verner, D. A., & Ferland, G. J. 1996, ApJS, 103, 467  
 Verner, D. A., & Yakovlev, D. G. 1995, A&AS, 109, 125  
 Zatsarinny, O., Gorczyca, T.W., Korista, K.T., Badnell, N.R., & Savin, D.W. 2004, A&A, 417, 1173; erratum, Zatsarinny, O., Gorczyca, T.W., Korista, K.T., Fu, J., Badnell, N.R., Mitthumsiri, W., & Savin, D.W. 2005, A&A, 440, 1203  
 Zatsarinny, O., Gorczyca, T.W., Fu, J., Korista, K.T., Badnell, N.R., & Savin, D.W. 2006, A&A, 447, 379

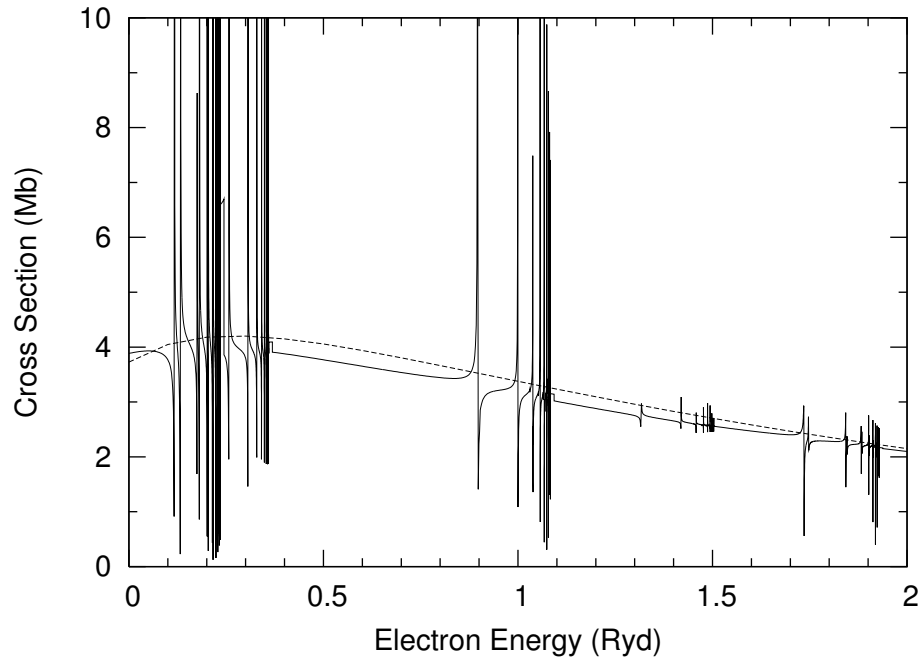


FIG. 1.— Photoionization:  $O(^3P) \rightarrow O^+(^4S)$ . Solid curve, *R*-matrix results (Butler & Zeppen 1990); dashed curve, present AUTOSTRUCTURE results.

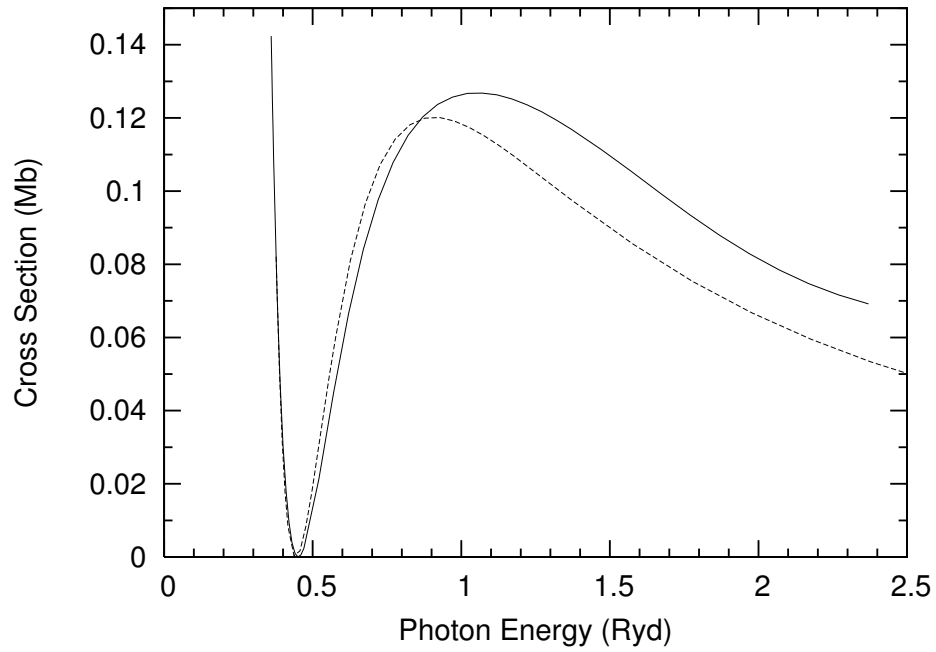


FIG. 2.— Photoionization of  $Na(3s)$ . Solid curve, *R*-matrix results (TOPbase, Cunto et al. 1993); dashed curve, present AUTOSTRUCTURE results.

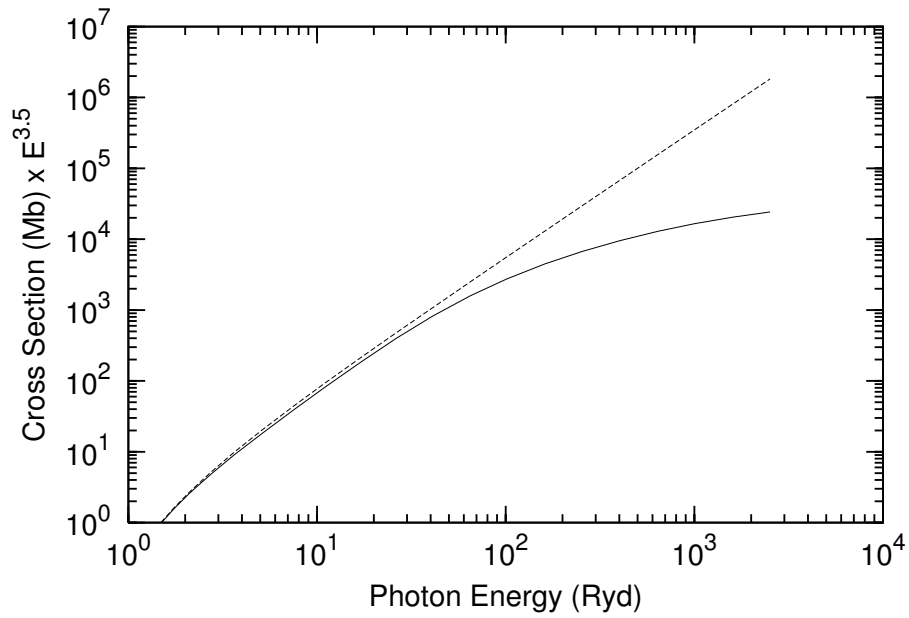


FIG. 3.— Scaled photoionization cross section of  $\text{Mg}^+(3s)$ . Solid curve, present AUTOSTRUCTURE results; dashed curve, Dirac-Hartree-Slater results of Verner & Yakovlev (1995).

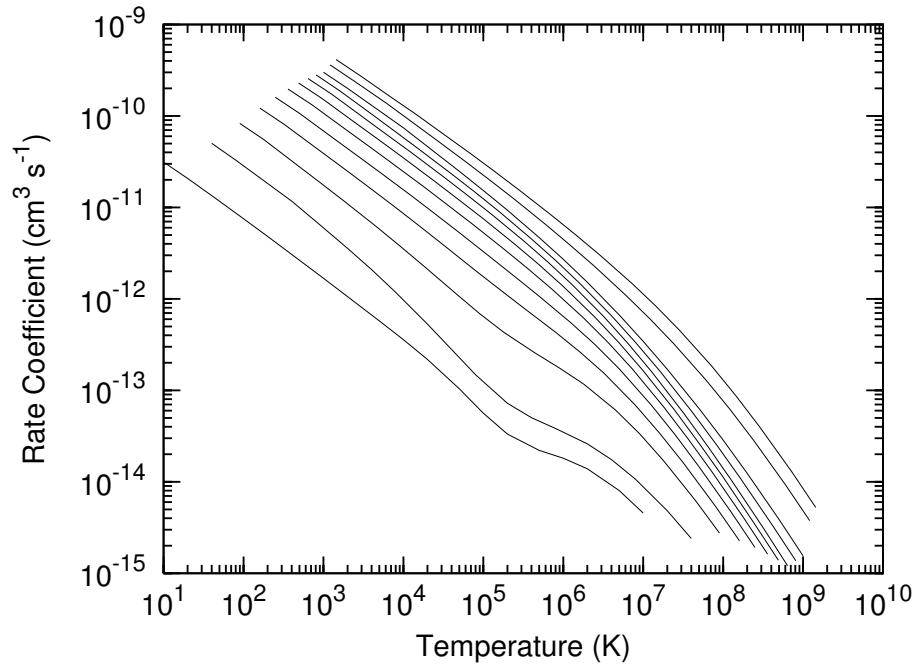


FIG. 4.— Total groundstate RR rate coefficients for the Mg isonuclear sequence (present AUTOSTRUCTURE results). Curves for singly ionized to bare are shown, moving left-to-right.

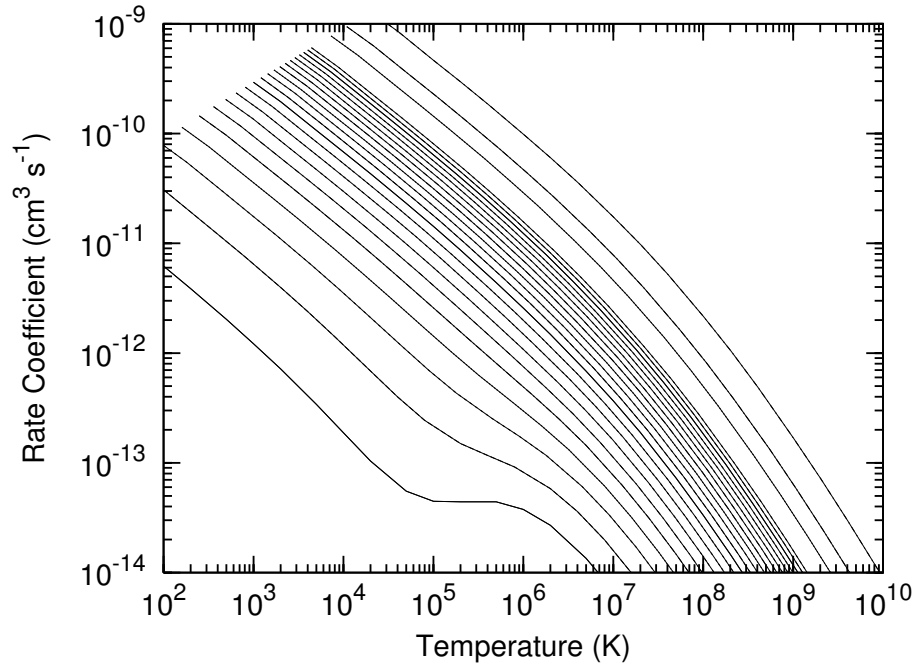


FIG. 5.— Total groundstate RR rate coefficients for the F isoelectronic sequence (present AUTOSTRUCTURE results). Curves for Ne to Zn, plus Kr, Mo, Xe are shown, moving left-to-right.

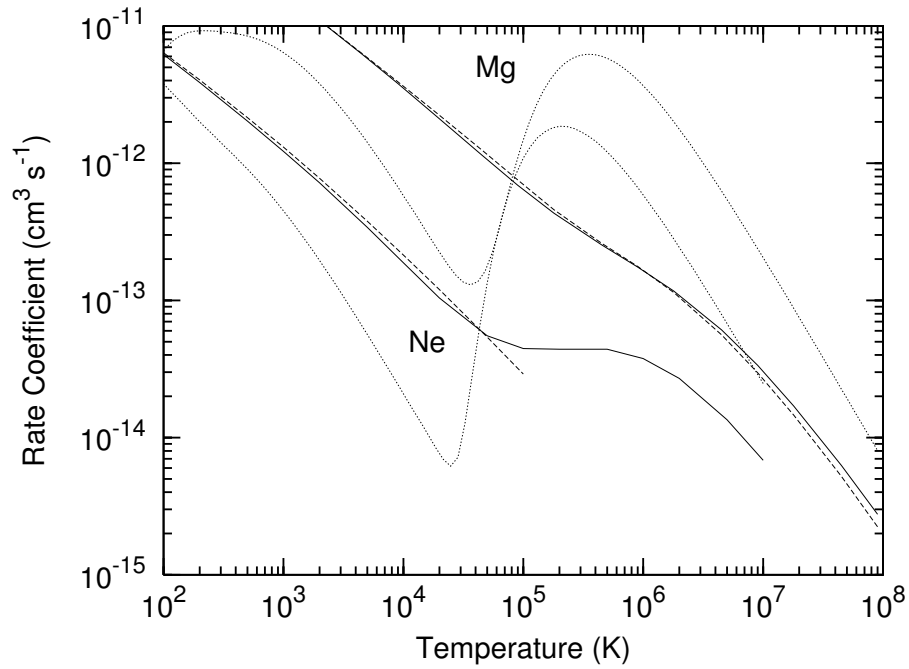


FIG. 6.— Total groundstate rate coefficients for F-like Ne and Mg. Solid curves, present AUTOSTRUCTURE RR results; dashed curves, RR results of Péquignot et al. (1991) and Gu (2003b) for Ne and Mg, respectively; dotted curves, DR results of Zatsarinny et al. (2006).

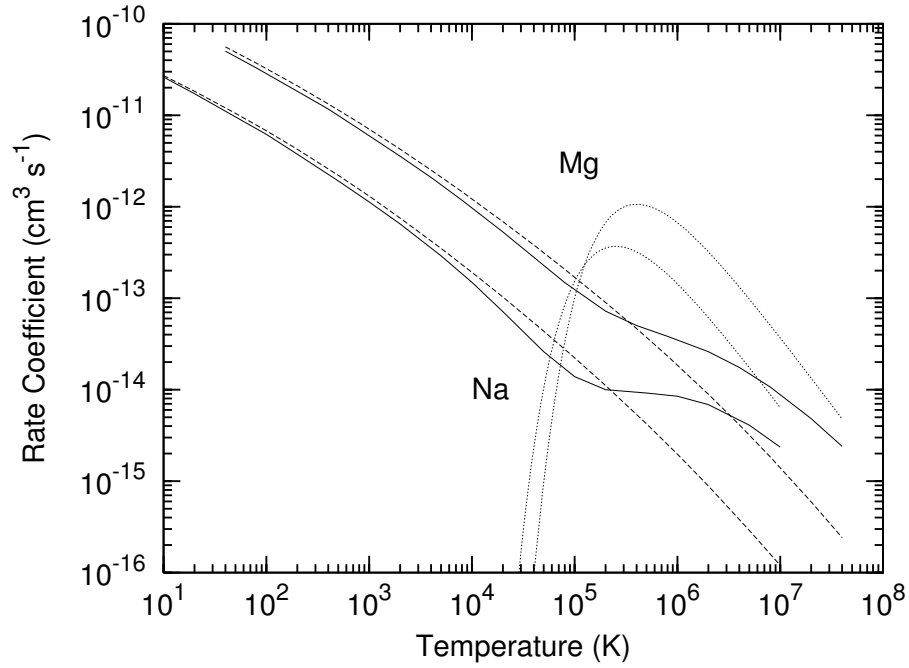


FIG. 7.— Total groundstate rate coefficients for Ne-like Na and Mg. Solid curves, present AUTOSTRUCTURE RR results; dashed curves, RR results of Verner & Ferland (1996); dotted curves, DR results of Gorczyca et al. (2006b) .

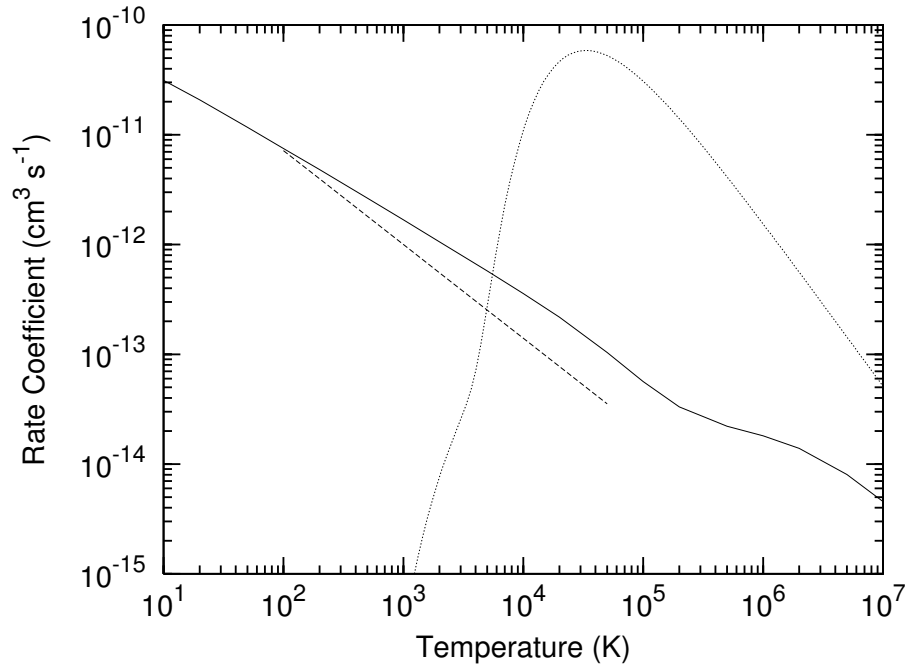


FIG. 8.— Total groundstate rate coefficients for  $\text{Mg}^+$ . Solid curves, present AUTOSTRUCTURE RR results; dashed curve, RR results of Aldrovandi & Péquignot (1973); dotted curves, DR results of Altun et al. (2006).



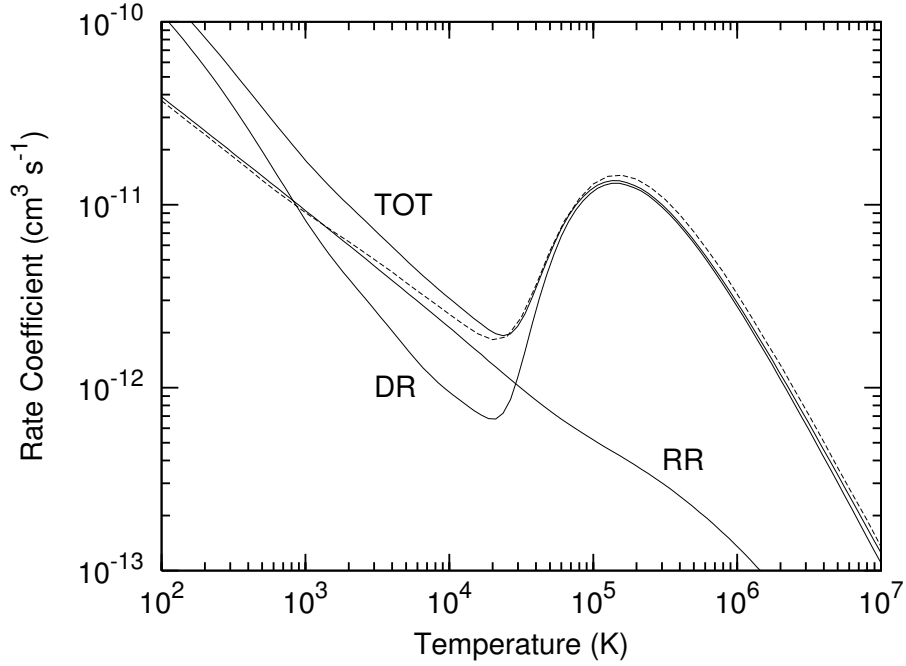


FIG. 9.— Total groundstate rate coefficients for  $O^{2+}$ . Solid curves, RR (present), DR (Zatsarinny et al. 2004a), and total (DR+RR) from AUTOSTRUCTURE; dashed curve, total from *R*-matrix (Nahar 1999).

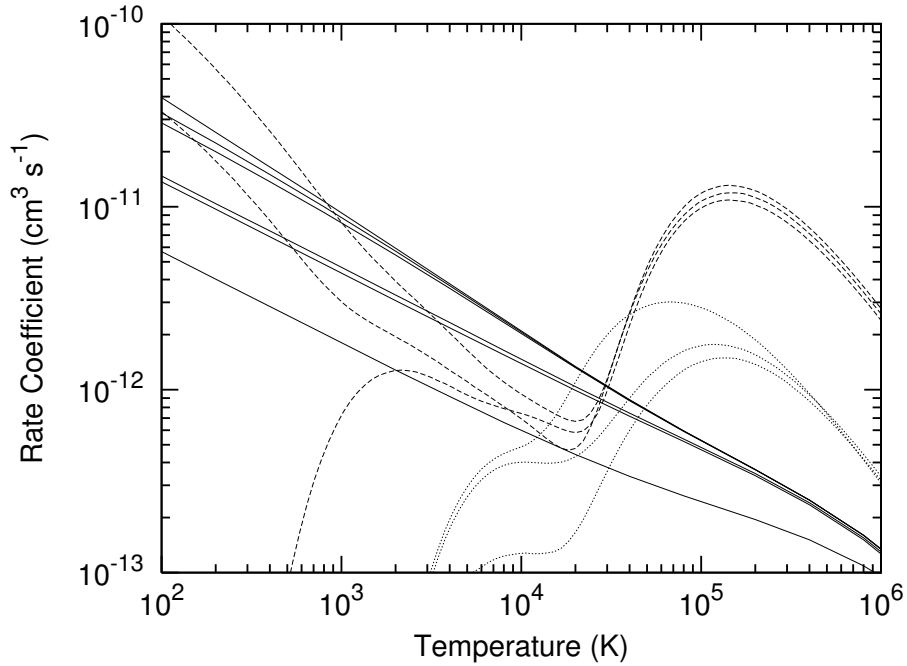


FIG. 10.— Total rate coefficients from the ground and metastable levels of  $O^{2+}$  ( $^3P_{0,1,2}, ^1D_2, ^1S_0, ^5S_2$ ). Solid curves, RR, top-to-bottom at  $10^5$  K corresponds to increasing initial energy metastable; dashed curves, DR from levels of the ground term, top-to-bottom corresponds to increasing initial energy metastable; dotted curves, DR from the excited terms, bottom-to-top at  $10^5$  K corresponds to increasing initial energy metastable. All DR taken from Badnell (2006a), based-on Zatsarinny et al. (2004a).

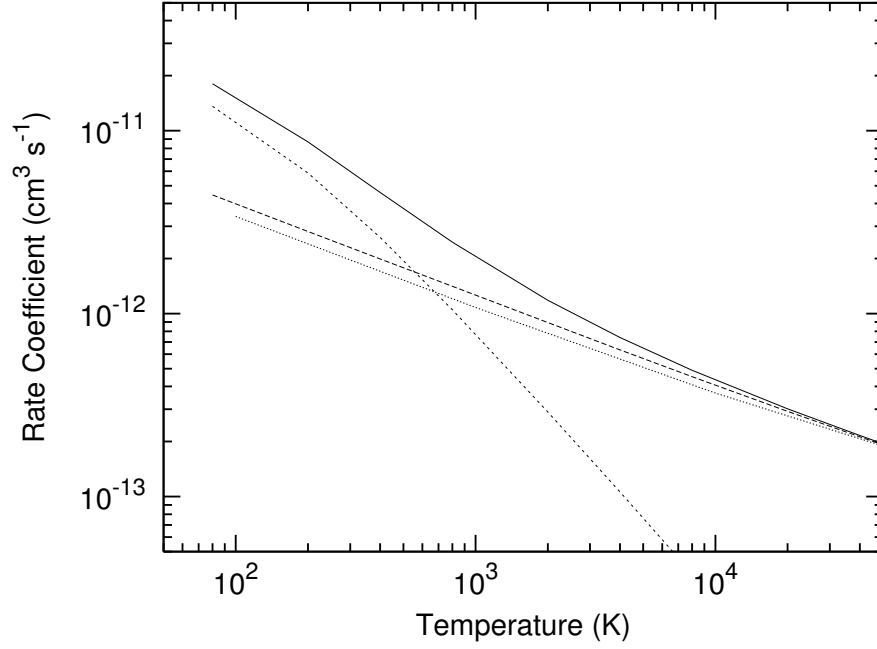


FIG. 11.— Partial recombination rate coefficients for  $O^{2+}$  to  $O^+$  groundstate-to-groundstate. Long-dashed curve, RR (present); short-dashed curve, DR (Zatsarinny et al. 2004a); solid curve, total (DR+RR); dotted curve,  $R$ -matrix (Nahar 1999).

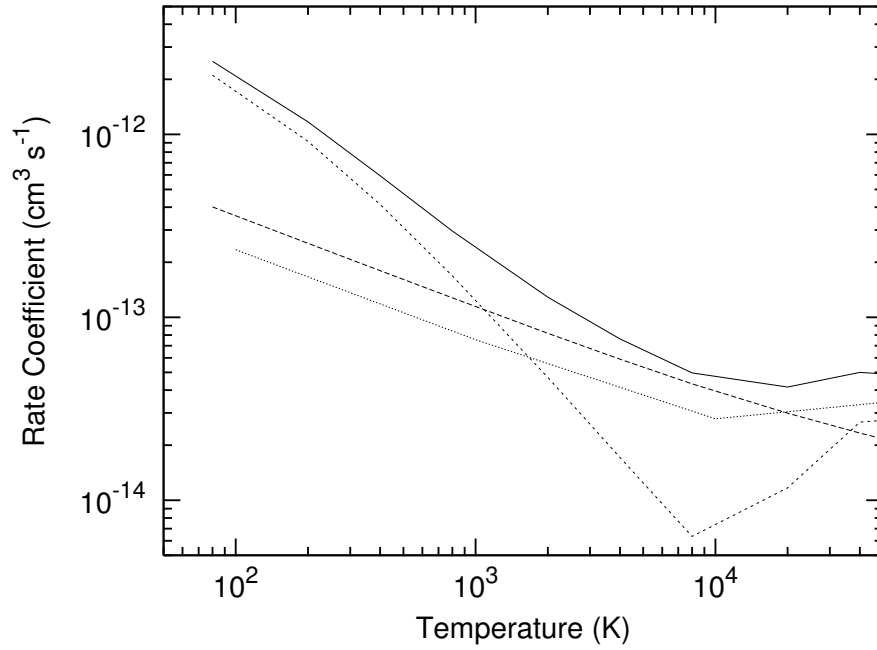


FIG. 12.— Partial recombination rate coefficients for  $O^{2+}$  groundstate to  $O^+$   $2s^2 2p^2 3p^4 D$ . Long-dashed curve, RR (present); short-dashed curve, DR (Zatsarinny et al. 2004a); solid curve, total (DR+RR); dotted curve,  $R$ -matrix (Nahar 1999).

TABLE 1  
FIT COEFFICIENTS FOR TOTAL GROUNDSTATE RR RATE COEFFICIENTS — SEE EQUATIONS (1) AND (2).  $Z$  DENOTES THE NUCLEAR CHARGE AND  $N$  THE NUMBER OF ELECTRONS ON THE ION BEFORE RECOMBINATION.

$Z$	$N$	$A$	$B$	$T_0$	$T_1$	$C$	$T_2$
1	0	8.318(-11) <sup>a</sup>	0.7472	2.965(0)	7.001(5)		
2	0	1.818(-10)	0.7492	1.017(1)	2.786(6)		
3	0	2.867(-10)	0.7493	2.108(1)	6.268(6)		
4	0	3.375(-10)	0.7475	4.628(1)	1.121(7)		
5	0	4.647(-10)	0.7484	6.142(1)	1.753(7)		
6	0	5.337(-10)	0.7485	9.502(1)	2.517(7)		
7	0	6.170(-10)	0.7481	1.316(2)	3.427(7)		
8	0	6.552(-10)	0.7470	1.951(2)	4.483(7)		
9	0	8.218(-10)	0.7491	2.046(2)	5.638(7)		
10	0	8.278(-10)	0.7470	2.991(2)	7.006(7)		
11	0	9.743(-10)	0.7488	3.217(2)	8.428(7)		
12	0	1.022(-09)	0.7476	4.098(2)	1.011(8)		
13	0	1.134(-09)	0.7482	4.619(2)	1.179(8)		
14	0	1.261(-09)	0.7488	5.068(2)	1.365(8)		
15	0	1.269(-09)	0.7472	6.495(2)	1.581(8)		
16	0	1.432(-09)	0.7485	6.688(2)	1.793(8)		
17	0	1.487(-09)	0.7489	7.847(2)	2.012(8)		
18	0	1.615(-09)	0.7483	8.433(2)	2.266(8)		
19	0	1.623(-09)	0.7473	1.024(3)	2.543(8)		
20	0	1.809(-09)	0.7490	1.025(3)	2.788(8)		
21	0	1.752(-09)	0.7470	1.303(3)	3.095(8)		
22	0	1.899(-09)	0.7476	1.348(3)	3.393(8)		
23	0	2.051(-09)	0.7490	1.389(3)	3.691(8)		
24	0	2.046(-09)	0.7476	1.638(3)	4.027(8)		
25	0	2.306(-09)	0.7499	1.546(3)	4.333(8)		
26	0	2.275(-09)	0.7481	1.836(3)	4.736(8)		
27	0	2.234(-09)	0.7461	2.190(3)	5.152(8)		
28	0	2.577(-09)	0.7497	1.949(3)	5.434(8)		
29	0	2.456(-09)	0.7477	2.414(3)	5.896(8)		
30	0	2.854(-09)	0.7491	2.125(3)	6.271(8)		
36	0	3.140(-09)	0.7485	3.537(3)	9.062(8)		
42	0	3.583(-09)	0.7474	5.008(3)	1.235(9)		
54	0	5.120(-09)	0.7493	6.912(3)	2.036(9)		
2	1	5.235(-11)	0.6988	7.301(0)	4.475(6)	0.0829	1.682(5)
3	1	9.349(-11)	0.6916	3.470(1)	7.329(6)	0.0351	6.293(5)
4	1	1.324(-10)	0.6806	8.525(1)	1.510(7)		
5	1	1.729(-10)	0.6776	1.552(2)	2.065(7)		
6	1	2.044(-10)	0.6742	2.647(2)	2.773(7)		
7	1	2.388(-10)	0.6732	3.960(2)	3.583(7)		
8	1	2.652(-10)	0.6705	5.842(2)	4.559(7)		
9	1	3.128(-10)	0.6712	7.227(2)	5.587(7)		
10	1	3.415(-10)	0.6706	9.552(2)	6.778(7)		
11	1	3.879(-10)	0.6718	1.133(3)	8.008(7)		
12	1	4.214(-10)	0.6713	1.396(3)	9.433(7)		
13	1	4.578(-10)	0.6707	1.673(3)	1.096(8)		
14	1	4.870(-10)	0.6697	2.026(3)	1.265(8)		
15	1	5.520(-10)	0.6724	2.146(3)	1.423(8)		
16	1	5.546(-10)	0.6692	2.754(3)	1.633(8)		
17	1	6.110(-10)	0.6712	2.956(3)	1.810(8)		
18	1	6.405(-10)	0.6698	3.425(3)	2.037(8)		
19	1	7.022(-10)	0.6721	3.602(3)	2.234(8)		
20	1	7.045(-10)	0.6693	4.391(3)	2.500(8)		
21	1	8.052(-10)	0.6750	4.198(3)	2.669(8)		
22	1	8.152(-10)	0.6728	4.937(3)	2.950(8)		
23	1	8.373(-10)	0.6711	5.622(3)	3.232(8)		
24	1	8.771(-10)	0.6722	6.118(3)	3.478(8)		
25	1	9.127(-10)	0.6717	6.691(3)	3.775(8)		
26	1	9.983(-10)	0.6754	6.651(3)	4.017(8)		
27	1	1.017(-09)	0.6738	7.469(3)	4.347(8)		
28	1	1.063(-09)	0.6744	7.979(3)	4.653(8)		
29	1	1.078(-09)	0.6736	8.924(3)	4.988(8)		
30	1	1.142(-09)	0.6750	9.193(3)	5.308(8)		
36	1	1.245(-09)	0.6716	1.601(4)	7.664(8)		
42	1	1.536(-09)	0.6764	2.012(4)	1.008(9)		
54	1	2.278(-09)	0.6872	2.680(4)	1.560(9)		
3	2	8.700(-12)	0.3640	1.470(2)	7.153(6)	0.1508	7.154(5)
4	2	1.861(-11)	0.4052	5.365(2)	2.254(7)		
5	2	3.251(-11)	0.4558	9.164(2)	1.749(7)		
6	2	4.798(-11)	0.4834	1.355(3)	1.872(7)		
7	2	6.245(-11)	0.4985	1.957(3)	2.177(7)		
8	2	8.193(-11)	0.5165	2.392(3)	2.487(7)		
9	2	9.958(-11)	0.5274	3.012(3)	2.896(7)		
10	2	1.186(-10)	0.5354	3.647(3)	3.365(7)		
11	2	1.393(-10)	0.5433	4.258(3)	3.872(7)		
12	2	1.602(-10)	0.5492	4.944(3)	4.434(7)		
13	2	1.761(-10)	0.5514	5.962(3)	5.081(7)		
14	2	2.017(-10)	0.5588	6.494(3)	5.693(7)		
15	2	2.190(-10)	0.5607	7.591(3)	6.396(7)		
16	2	2.362(-10)	0.5615	8.776(3)	7.208(7)		
17	2	2.594(-10)	0.5663	9.623(3)	7.952(7)		
18	2	2.812(-10)	0.5686	1.063(4)	8.779(7)		
19	2	3.046(-10)	0.5712	1.160(4)	9.639(7)		
20	2	3.250(-10)	0.5743	1.276(4)	1.051(8)		
21	2	3.366(-10)	0.5721	1.473(4)	1.163(8)		
22	2	3.658(-10)	0.5767	1.540(4)	1.250(8)		
23	2	3.815(-10)	0.5761	1.718(4)	1.368(8)		
24	2	3.963(-10)	0.5760	1.914(4)	1.479(8)		
25	2	4.386(-10)	0.5838	1.888(4)	1.556(8)		
26	2	4.458(-10)	0.5802	2.155(4)	1.701(8)		
27	2	4.629(-10)	0.5805	2.352(4)	1.831(8)		
28	2	4.901(-10)	0.5836	2.460(4)	1.937(8)		
29	2	5.041(-10)	0.5828	2.701(4)	2.082(8)		
30	2	5.258(-10)	0.5832	2.882(4)	2.221(8)		
36	2	6.300(-10)	0.5851	4.346(4)	3.140(8)		
42	2	8.161(-10)	0.5972	5.082(4)	4.054(8)		
54	2	1.082(-09)	0.6049	8.335(4)	6.391(8)		
4	3	1.793(-10)	0.7669	8.938(-01)	2.138(6)	0.0310	1.382(4)
5	3	3.417(-10)	0.7512	3.604(0)	2.821(6)	0.0351	1.295(7)
6	3	1.120(-10)	0.6737	1.115(2)	5.938(6)		
7	3	1.533(-10)	0.6682	1.823(2)	7.751(6)		
8	3	1.724(-10)	0.6556	3.372(2)	1.030(7)		
9	3	2.244(-10)	0.6574	4.147(2)	1.268(7)		
10	3	2.755(-10)	0.6586	5.102(2)	1.535(7)		
11	3	3.171(-10)	0.6576	6.526(2)	1.848(7)		
12	3	3.445(-10)	0.6553	8.693(2)	2.196(7)		
13	3	3.916(-10)	0.6565	1.025(3)	2.544(7)		

TABLE 1 — *Continued*

<i>Z</i>	<i>N</i>	<i>A</i>	<i>B</i>	<i>T</i> <sub>0</sub>	<i>T</i> <sub>1</sub>	<i>C</i>	<i>T</i> <sub>2</sub>
14	3	4.633(-10)	0.6602	1.088(3)	2.896(7)		
15	3	4.972(-10)	0.6581	1.329(3)	3.346(7)		
16	3	5.511(-10)	0.6598	1.492(3)	3.755(7)		
17	3	6.038(-10)	0.6611	1.670(3)	4.213(7)		
18	3	6.557(-10)	0.6624	1.868(3)	4.693(7)		
19	3	7.052(-10)	0.6613	2.094(3)	5.246(7)		
20	3	7.848(-10)	0.6644	2.173(3)	5.749(7)		
21	3	8.463(-10)	0.6653	2.355(3)	6.304(7)		
22	3	9.040(-10)	0.6666	2.565(3)	6.864(7)		
23	3	9.483(-10)	0.6655	2.859(3)	7.531(7)		
24	3	9.718(-10)	0.6643	3.285(3)	8.221(7)		
25	3	1.065(-09)	0.6668	3.327(3)	8.827(7)		
26	3	1.186(-09)	0.6713	3.253(3)	9.392(7)		
27	3	1.181(-09)	0.6681	3.839(3)	1.023(8)		
28	3	1.259(-09)	0.6699	3.991(3)	1.094(8)		
29	3	1.249(-09)	0.6668	4.697(3)	1.181(8)		
30	3	1.381(-09)	0.6705	4.543(3)	1.249(8)		
36	3	1.674(-09)	0.6723	6.836(3)	1.776(8)		
42	3	1.926(-09)	0.6717	9.982(3)	2.408(8)		
54	3	2.883(-09)	0.6818	1.355(4)	3.811(8)		
5	4	1.998(-09)	0.8277	1.269(-02)	1.016(6)	0.0901	3.058(4)
6	4	2.067(-09)	0.8012	1.643(-01)	2.172(6)	0.0427	6.341(4)
7	4	7.923(-10)	0.7768	3.750(0)	3.468(6)	0.0223	7.206(4)
8	4	3.955(-09)	0.7813	6.821(-01)	5.076(6)		
9	4	3.298(-09)	0.7702	2.103(0)	6.441(6)		
10	4	2.557(-09)	0.7601	6.293(0)	8.091(6)		
11	4	1.654(-09)	0.7508	2.276(1)	9.950(6)		
12	4	3.989(-10)	1.0231	2.601(1)	1.227(7)		
13	4	1.578(-09)	0.7394	6.157(1)	1.427(7)		
14	4	1.851(-09)	0.7384	6.906(1)	1.644(7)		
15	4	1.543(-09)	0.7315	1.330(2)	1.926(7)		
16	4	1.740(-09)	0.7303	1.494(2)	2.193(7)		
17	4	2.027(-09)	0.7307	1.541(2)	2.470(7)		
18	4	2.165(-09)	0.7307	1.801(2)	2.753(7)		
19	4	2.224(-09)	0.7299	2.212(2)	3.069(7)		
20	4	2.421(-09)	0.7278	2.438(2)	3.424(7)		
21	4	2.253(-09)	0.7253	3.425(2)	3.802(7)		
22	4	2.463(-09)	0.7249	3.638(2)	4.164(7)		
23	4	2.660(-09)	0.7253	3.897(2)	4.538(7)		
24	4	2.747(-09)	0.7251	4.436(2)	4.921(7)		
25	4	2.589(-09)	0.7216	5.887(2)	5.400(7)		
26	4	3.322(-09)	0.7264	4.563(2)	5.746(7)		
27	4	3.885(-09)	0.7301	4.100(2)	6.101(7)		
28	4	3.531(-09)	0.7260	5.650(2)	6.627(7)		
29	4	3.862(-09)	0.7272	5.631(2)	7.100(7)		
30	4	4.233(-09)	0.7283	5.568(2)	7.545(7)		
36	4	4.645(-09)	0.7261	1.018(3)	1.083(8)		
42	4	6.974(-09)	0.7318	9.622(2)	1.438(8)		
54	4	1.052(-08)	0.7363	1.319(3)	2.321(8)		
6	5	2.995(-09)	0.7849	6.670(-03)	1.943(6)	0.1597	4.955(4)
7	5	2.410(-09)	0.7948	1.231(-01)	3.016(6)	0.0774	1.016(5)
8	5	2.501(-09)	0.7844	5.235(-01)	4.470(6)	0.0447	1.642(5)
9	5	2.236(-09)	0.7725	1.828(0)	5.982(6)	0.0319	2.529(5)
10	5	1.127(-09)	0.7556	1.311(1)	8.047(6)	0.0250	2.771(5)
11	5	4.040(-09)	0.7665	2.908(0)	1.043(7)		
12	5	3.859(-09)	0.7579	5.587(0)	1.235(7)		
13	5	2.284(-09)	0.7480	2.178(1)	1.460(7)		
14	5	1.688(-09)	0.7390	5.549(1)	1.716(7)		
15	5	1.948(-09)	0.7375	6.372(1)	1.947(7)		
16	5	1.702(-09)	0.7301	1.138(2)	2.253(7)		
17	5	1.655(-09)	0.7262	1.636(2)	2.543(7)		
18	5	1.780(-09)	0.7252	1.933(2)	2.837(7)		
19	5	2.079(-09)	0.7245	1.954(2)	3.156(7)		
20	5	2.019(-09)	0.7215	2.644(2)	3.506(7)		
21	5	2.055(-09)	0.7200	3.236(2)	3.860(7)		
22	5	1.959(-09)	0.7169	4.381(2)	4.258(7)		
23	5	2.131(-09)	0.7166	4.679(2)	4.637(7)		
24	5	2.302(-09)	0.7167	5.002(2)	5.030(7)		
25	5	2.450(-09)	0.7160	5.442(2)	5.456(7)		
26	5	2.199(-09)	0.7118	7.810(2)	5.946(7)		
27	5	2.654(-09)	0.7148	6.726(2)	6.351(7)		
28	5	2.660(-09)	0.7150	7.865(2)	6.761(7)		
29	5	2.679(-09)	0.7128	9.094(2)	7.300(7)		
30	5	2.916(-09)	0.7150	9.113(2)	7.726(7)		
36	5	3.422(-09)	0.7122	1.533(3)	1.107(8)		
42	5	4.461(-09)	0.7147	1.874(3)	1.481(8)		
54	5	5.917(-09)	0.7162	3.263(3)	2.390(8)		
7	6	6.387(-10)	0.7308	9.467(-02)	2.954(6)	0.2440	6.739(4)
8	6	2.096(-09)	0.7668	1.602(-01)	4.377(6)	0.1070	1.392(5)
9	6	1.468(-09)	0.7652	1.284(0)	6.039(6)	0.0664	2.235(5)
10	6	1.861(-09)	0.7593	2.504(0)	8.037(6)	0.0406	3.255(5)
11	6	1.077(-09)	0.7469	1.430(1)	1.018(7)	0.0289	3.593(5)
12	6	9.133(-10)	0.7353	3.674(1)	1.263(7)	0.0211	4.049(5)
13	6	4.100(-09)	0.7507	5.134(0)	1.603(7)		
14	6	2.100(-09)	0.7401	2.523(1)	1.842(7)		
15	6	1.763(-09)	0.7310	5.234(1)	2.117(7)		
16	6	1.518(-09)	0.7246	9.845(1)	2.390(7)		
17	6	1.440(-09)	0.7187	1.522(2)	2.712(7)		
18	6	1.464(-09)	0.7144	2.040(2)	3.025(7)		
19	6	1.461(-09)	0.7108	2.734(2)	3.371(7)		
20	6	1.532(-09)	0.7089	3.305(2)	3.713(7)		
21	6	1.432(-09)	0.7048	4.761(2)	4.102(7)		
22	6	1.458(-09)	0.7005	5.875(2)	4.526(7)		
23	6	1.532(-09)	0.7008	6.698(2)	4.908(7)		
24	6	1.567(-09)	0.6986	7.957(2)	5.340(7)		
25	6	1.642(-09)	0.6982	8.948(2)	5.767(7)		
26	6	1.659(-09)	0.6958	1.061(3)	6.253(7)		
27	6	1.672(-09)	0.6935	1.254(3)	6.763(7)		
28	6	1.744(-09)	0.6928	1.385(3)	7.245(7)		
29	6	2.128(-09)	0.6988	1.157(3)	7.589(7)		
30	6	1.805(-09)	0.6906	1.794(3)	8.293(7)		
36	6	2.330(-09)	0.6908	2.631(3)	1.171(8)		
42	6	2.791(-09)	0.6893	3.801(3)	1.583(8)		
54	6	3.626(-09)	0.6904	6.985(3)	2.542(8)		
8	7	6.622(-11)	0.6109	4.136(0)	4.214(6)	0.4093	8.770(4)
9	7	5.595(-10)	0.7083	1.462(0)	6.258(6)	0.1645	1.880(5)
10	7	8.321(-10)	0.7254	3.332(0)	8.696(6)	0.0921	3.044(5)
11	7	1.087(-09)	0.7284	6.132(0)	1.088(7)	0.0629	4.559(5)

TABLE 1 — *Continued*

<i>Z</i>	<i>N</i>	<i>A</i>	<i>B</i>	<i>T</i> <sub>0</sub>	<i>T</i> <sub>1</sub>	<i>C</i>	<i>T</i> <sub>2</sub>
12	7	7.515(-10)	0.7203	2.582(1)	1.355(7)	0.0436	5.691(5)
13	7	7.728(-10)	0.7152	4.818(1)	1.672(7)	0.0271	7.209(5)
14	7	7.532(-10)	0.7072	8.860(1)	1.997(7)	0.0185	6.949(5)
15	7	1.570(-09)	0.7190	4.177(1)	2.438(7)		
16	7	1.137(-09)	0.7080	1.099(2)	2.745(7)		
17	7	1.146(-09)	0.7033	1.593(2)	3.034(7)		
18	7	1.022(-09)	0.6948	2.747(2)	3.391(7)		
19	7	9.722(-10)	0.6898	4.087(2)	3.753(7)		
20	7	9.575(-10)	0.6843	5.634(2)	4.150(7)		
21	7	1.011(-09)	0.6827	6.726(2)	4.518(7)		
22	7	1.043(-09)	0.6798	8.226(2)	4.947(7)		
23	7	1.049(-09)	0.6763	1.032(3)	5.381(7)		
24	7	1.053(-09)	0.6736	1.278(3)	5.857(7)		
25	7	1.089(-09)	0.6713	1.488(3)	6.327(7)		
26	7	1.135(-09)	0.6705	1.691(3)	6.809(7)		
27	7	1.177(-09)	0.6687	1.921(3)	7.331(7)		
28	7	1.172(-09)	0.6652	2.320(3)	7.926(7)		
29	7	1.295(-09)	0.6672	2.319(3)	8.388(7)		
30	7	1.250(-09)	0.6640	2.899(3)	8.992(7)		
36	7	1.497(-09)	0.6596	4.992(3)	1.277(8)		
42	7	1.748(-09)	0.6593	7.627(3)	1.705(8)		
54	7	2.624(-09)	0.6641	1.134(4)	2.699(8)		
9	8	3.769(-11)	0.5559	1.091(1)	6.413(6)	0.4534	1.095(5)
10	8	1.773(-10)	0.6434	9.924(0)	8.878(6)	0.2205	2.292(5)
11	8	3.192(-10)	0.6726	1.640(1)	1.263(7)	0.1232	3.725(5)
12	8	4.031(-10)	0.6803	3.205(1)	1.626(7)	0.0764	5.399(5)
13	8	4.438(-10)	0.6789	6.204(1)	1.940(7)	0.0571	7.410(5)
14	8	4.615(-10)	0.6753	1.143(2)	2.377(7)	0.0356	8.595(5)
15	8	5.508(-10)	0.6748	1.501(2)	2.772(7)	0.0213	1.109(6)
16	8	8.773(-10)	0.6853	1.115(2)	3.386(7)		
17	8	7.522(-10)	0.6767	2.213(2)	3.678(7)		
18	8	6.805(-10)	0.6667	3.866(2)	4.062(7)		
19	8	6.633(-10)	0.6599	5.735(2)	4.447(7)		
20	8	6.699(-10)	0.6546	7.761(2)	4.861(7)		
21	8	6.581(-10)	0.6494	1.072(3)	5.292(7)		
22	8	6.854(-10)	0.6464	1.313(3)	5.733(7)		
23	8	7.140(-10)	0.6441	1.579(3)	6.195(7)		
24	8	6.832(-10)	0.6367	2.162(3)	6.770(7)		
25	8	7.236(-10)	0.6359	2.448(3)	7.264(7)		
26	8	7.556(-10)	0.6351	2.800(3)	7.742(7)		
27	8	7.582(-10)	0.6307	3.402(3)	8.406(7)		
28	8	7.889(-10)	0.6292	3.842(3)	8.956(7)		
29	8	8.107(-10)	0.6290	4.369(3)	9.503(7)		
30	8	8.533(-10)	0.6278	4.759(3)	1.011(8)		
36	8	1.033(-09)	0.6234	8.342(3)	1.417(8)		
42	8	1.256(-09)	0.6232	1.220(4)	1.882(8)		
54	8	1.688(-09)	0.6241	2.245(4)	2.986(8)		
10	9	1.295(-11)	0.3556	6.739(1)	7.563(6)	0.6472	1.598(5)
11	9	5.176(-11)	0.4811	7.751(1)	1.351(7)	0.3467	3.140(5)
12	9	1.249(-10)	0.5600	7.748(1)	2.015(7)	0.1917	5.139(5)
13	9	2.011(-10)	0.5984	1.013(2)	2.635(7)	0.1072	7.591(5)
14	9	2.468(-10)	0.6113	1.649(2)	3.231(7)	0.0636	9.837(5)
15	9	2.981(-10)	0.6173	2.372(2)	3.807(7)	0.0361	1.306(6)
16	9	3.384(-10)	0.6175	3.380(2)	4.347(7)	0.0225	1.672(6)
17	9	4.354(-10)	0.6262	3.604(2)	5.251(7)		
18	9	4.228(-10)	0.6181	5.880(2)	5.535(7)		
19	9	4.044(-10)	0.6099	9.347(2)	5.922(7)		
20	9	3.992(-10)	0.6025	1.362(3)	6.373(7)		
21	9	4.070(-10)	0.5968	1.819(3)	6.864(7)		
22	9	4.281(-10)	0.5954	2.234(3)	7.270(7)		
23	9	4.227(-10)	0.5885	3.007(3)	7.863(7)		
24	9	4.341(-10)	0.5846	3.714(3)	8.452(7)		
25	9	4.710(-10)	0.5863	4.081(3)	8.874(7)		
26	9	4.791(-10)	0.5823	4.967(3)	9.535(7)		
27	9	5.045(-10)	0.5808	5.617(3)	1.015(8)		
28	9	5.081(-10)	0.5766	6.786(3)	1.088(8)		
29	9	5.402(-10)	0.5769	7.375(3)	1.150(8)		
30	9	5.284(-10)	0.5705	9.182(3)	1.239(8)		
36	9	6.842(-10)	0.5709	1.489(4)	1.680(8)		
42	9	8.282(-10)	0.5708	2.249(4)	2.193(8)		
54	9	1.109(-09)	0.5712	4.285(4)	3.443(8)		
11	10	5.095(-12)	0.0000	3.546(2)	2.310(6)	0.9395	4.297(5)
12	10	1.345(-11)	0.1074	7.877(2)	7.925(7)	0.4631	5.027(5)
13	10	3.107(-11)	0.2854	8.207(2)	8.117(7)	0.2631	7.693(5)
14	10	5.134(-11)	0.3678	1.009(3)	8.514(7)	0.1646	1.084(6)
15	10	7.550(-11)	0.4244	1.206(3)	8.603(7)	0.1008	1.498(6)
16	10	9.565(-11)	0.4517	1.599(3)	9.252(7)	0.0612	1.986(6)
17	10	1.144(-10)	0.4665	2.108(3)	9.895(7)	0.0362	2.397(6)
18	10	1.313(-10)	0.4722	2.767(3)	1.066(8)	0.0208	2.725(6)
19	10	1.590(-10)	0.4867	3.096(3)	1.192(8)		
20	10	1.622(-10)	0.4804	4.449(3)	1.204(8)		
21	10	1.647(-10)	0.4734	6.182(3)	1.253(8)		
22	10	1.730(-10)	0.4687	7.898(3)	1.302(8)		
23	10	1.800(-10)	0.4650	9.950(3)	1.357(8)		
24	10	1.868(-10)	0.4603	1.233(4)	1.432(8)		
25	10	1.924(-10)	0.4562	1.514(4)	1.509(8)		
26	10	2.034(-10)	0.4548	1.751(4)	1.579(8)		
27	10	2.125(-10)	0.4518	2.042(4)	1.667(8)		
28	10	2.208(-10)	0.4504	2.355(4)	1.749(8)		
29	10	2.271(-10)	0.4464	2.753(4)	1.853(8)		
30	10	2.397(-10)	0.4458	3.040(4)	1.941(8)		
36	10	3.051(-10)	0.4446	5.297(4)	2.530(8)		
42	10	3.541(-10)	0.4350	8.882(4)	3.334(8)		
54	10	4.923(-10)	0.4400	1.645(5)	5.012(8)		
12	11	5.452(-11)	0.6845	5.637(0)	1.551(6)	0.3945	8.360(5)
13	11	3.171(-11)	0.4493	1.821(2)	3.529(7)	0.2642	7.190(5)
14	11	6.739(-11)	0.4931	2.166(2)	4.491(7)	0.1667	9.046(5)
15	11	1.128(-10)	0.5330	2.618(2)	4.963(7)	0.0994	1.244(6)
16	11	1.588(-10)	0.5584	3.350(2)	5.188(7)	0.0591	1.656(6)
17	11	1.790(-10)	0.5641	5.390(2)	5.733(7)	0.0340	2.038(6)
18	11	2.156(-10)	0.5708	7.027(2)	6.146(7)	0.0169	2.845(6)
19	11	2.516(-10)	0.5771	8.854(2)	6.829(7)		
20	11	2.527(-10)	0.5711	1.364(3)	6.926(7)		
21	11	2.578(-10)	0.5655	1.955(3)	7.157(7)		
22	11	2.711(-10)	0.5628	2.552(3)	7.416(7)		
23	11	2.792(-10)	0.5588	3.360(3)	7.736(7)		
24	11	3.003(-10)	0.5585	3.987(3)	8.062(7)		
25	11	3.197(-10)	0.5582	4.712(3)	8.394(7)		

TABLE 1 — *Continued*

$Z$	$N$	$A$	$B$	$T_0$	$T_1$	$C$	$T_2$
26	11	3.133(-10)	0.5507	6.295(3)	9.035(7)		
27	11	3.340(-10)	0.5516	7.145(3)	9.384(7)		
28	11	3.626(-10)	0.5536	7.769(3)	9.785(7)		
29	11	3.761(-10)	0.5509	9.021(3)	1.036(8)		
30	11	3.885(-10)	0.5492	1.041(4)	1.095(8)		
36	11	4.936(-10)	0.5469	1.900(4)	1.455(8)		
42	11	6.295(-10)	0.5525	2.751(4)	1.846(8)		
54	11	8.258(-10)	0.5485	5.795(4)	2.911(8)		

<sup>a</sup> Note,  $x.y(n)$  denotes  $x.y \times 10^n$ .